



# A theoretical study of crystallochromy: Spectral tuning of solid-state tetracenes

Fujimoto, Kazuhiro.J  
Kitamura, Chitoshi

---

(Citation)

Journal of Chemical Physics, 139(8):084511-084511

(Issue Date)

2013-08-30

(Resource Type)

journal article

(Version)

Version of Record

(URL)

<https://hdl.handle.net/20.500.14094/90001854>





## A theoretical study of crystallochromy: Spectral tuning of solid-state tetracenes

Kazuhiro J. Fujimoto and Chitoshi Kitamura

Citation: *J. Chem. Phys.* **139**, 084511 (2013); doi: 10.1063/1.4819133

View online: <http://dx.doi.org/10.1063/1.4819133>

View Table of Contents: <http://jcp.aip.org/resource/1/JCPSA6/v139/i8>

Published by the AIP Publishing LLC.

---

### Additional information on J. Chem. Phys.


Journal Homepage: <http://jcp.aip.org/>

Journal Information: [http://jcp.aip.org/about/about\\_the\\_journal](http://jcp.aip.org/about/about_the_journal)

Top downloads: [http://jcp.aip.org/features/most\\_downloaded](http://jcp.aip.org/features/most_downloaded)

Information for Authors: <http://jcp.aip.org/authors>


## ADVERTISEMENT



# AIP | Applied Physics Letters

Accepting Submissions in  
Biophysics and Bio-Inspired Systems

*Submit Today*





## A theoretical study of crystallochromy: Spectral tuning of solid-state tetracenes

Kazuhiro J. Fujimoto<sup>1,a)</sup> and Chitoshi Kitamura<sup>2</sup>

<sup>1</sup>Department of Computational Science, Graduate School of System Informatics, Kobe University, 1-1 Rokkodai, Nada, Kobe 657-8501, Japan

<sup>2</sup>Department of Materials Science, School of Engineering, The University of Shiga Prefecture, 2500 Hassaka-cho, Hikone, Shiga 522-8533, Japan

(Received 16 June 2013; accepted 31 July 2013; published online 30 August 2013)

The crystallochromy of the red and yellow solids of tetracenes was theoretically investigated using the transition-density-fragment interaction combined with transfer integral method [K. J. Fujimoto, *J. Chem. Phys.* **137**, 034101 (2012)]. The calculated absorption and fluorescence energies were in good agreement with the experimental values for both solids. The spectral tuning mechanism was analyzed in terms of three contributions: side-chain conformational effect, electrostatic solid-state effect, and multimerization effect. This analysis provided an insight into the mechanism of the large spectral shift between the two solids. The multimerization effect was found to be primarily important for the large red-shift of the red solid. Further analysis also revealed the strong dependence of the excited state character on the molecular displacement. Such dependence was found to have a significant influence on the magnitudes of the absorption energy and oscillator strength. These results indicated that the present approach is useful for analyzing and understanding the mechanism of crystallochromy. © 2013 AIP Publishing LLC. [<http://dx.doi.org/10.1063/1.4819133>]

### I. INTRODUCTION

Crystallochromy<sup>1</sup> is a phenomenon of spectral shift induced by molecular aggregation,<sup>2</sup> and it is observed in solid state such as molecular crystal. This phenomenon was first found in 1907 by Hantzsch, who named it “chromoisomerism”.<sup>3,4</sup> This term has been superseded by “crystallochromy” which was first used in a study by Klebe *et al.*<sup>1</sup> describing perylene-bis(dicarboximide) pigments. In the synthetic dye industry, crystallochromy has often been referred to as “polymorphism.”<sup>5</sup> One example of crystallochromy is copper phthalocyanine (color index generic name: Pigment Blue 15),<sup>6</sup> which forms two types of crystal structures, an  $\alpha$  and a  $\beta$  packed form. Each exhibits a characteristic color, reddish blue in the case of the  $\alpha$ -form and greenish blue for the  $\beta$ -form.<sup>7</sup> The individual colors are widely used in inks, coatings, and plastics. Although the above pigments have the same molecular composition, they show different colors depending on the molecular packing arrangement in solid state. Here, it should be noted that the so-called “conformational polymorphism,”<sup>8</sup> which is a spectral shift phenomenon caused by a single-bond rotation of  $\pi$ -conjugation, is distinguished from crystallochromy in this article. Despite these early reports, detailed experimental analysis of crystallochromy has not yet been performed, due to the difficulty in observing solid-state spectra. In contrast, experiments on spectral shift in solution (i.e., solvatochromism) have been more extensive, and mechanism is better understood.<sup>9</sup> This is likely due to the more easily interpretable results obtained from these experiments.

To clarify the mechanism of crystallochromy, several theoretical models have been developed. McRae and Kasha proposed a simple interaction model based on molecular exciton theory using the point dipole approximation.<sup>10</sup> This gave an intuitive interpretation of the spectral shift attributed to the geometrical arrangement of molecules, such as that observed in J and H aggregates.<sup>2,11,12</sup> This model has been widely used for analyzing the alignment of molecules because of its simplicity. However, the utility of this model is limited to monolayer assemblies. To circumvent this problem, an extended dipole model was proposed by Czikkely *et al.*<sup>13</sup> This model successfully explained the spectral shift on the brick stone arrangement of cyanine pigments. Subsequently, the extended dipole model was generalized by Nagamura and Kamata, as applicable to the three-dimensional arrangement of molecules.<sup>14</sup> All three models are based on the Frenkel exciton model,<sup>15</sup> so that electronic coupling on the Coulomb interaction between two molecules plays a significant role in the spectral shift. In 1994, Kzmaier and Hoffmann presented an alternative view of the mechanism of crystallochromy.<sup>16</sup> They focused on intermolecular orbital interactions and clearly showed the importance of quantum-mechanical interference effects on crystallochromy. Since intermolecular orbital interactions are strongly related to electronic couplings on electron-transfer (ET), hole-transfer (HT), and charge-transfer (CT) interactions,<sup>17</sup> electronic couplings not only on the Coulomb interaction but also on the ET, HT, and CT interactions were indicated to be important for crystallochromy. In this meaning, their work gave a new insight into crystallochromy.

A similar history can be found in the study of excitation-energy transfer (EET). In general, the mechanism of EET

<sup>a)</sup>Electronic mail: [fujimoto@ruby.kobe-u.ac.jp](mailto:fujimoto@ruby.kobe-u.ac.jp)



is explained by Förster<sup>18</sup> and Dexter<sup>19</sup> theories, in which electronic couplings are based on the Coulomb and exchange interactions between two chromophores. In contrast, Harcourt *et al.* presented a significant influence of CT states on the EET process.<sup>20</sup> In their theory, electronic coupling was described with two kinds of configurations. One is the local excitations (LE) within a chromophore, and the other is the CT states between two chromophores. Since the Förster and Dexter theories were based only on the LE states, the admixture of CT states provided a general framework for electronic coupling.

Recently, one of the authors (C.K.) and his co-workers synthesized a series of 1, 4, 7, 10-tetraalkyltetracenes. By changing the length of the alkyl side-chain, the solid-state colors of tetracenes could be varied, ranging from yellow to orange to red.<sup>21</sup> Interestingly, both yellow (BUY) and red (BUR) solids were obtained from the butyl derivative. As a result of x-ray analysis, individual solids were confirmed to form different molecular packing structures. Thus, the difference in the solid-state colors was considered to result from crystallochromy. To understand the mechanism, a molecular exciton model was employed, with the point dipole approximation. However, this analysis was insufficient to achieve any qualitative understanding. Two reasons were considered; one is the problem of accuracy in the point dipole approximation, alternatively, the lack of consideration of other electronic couplings (i.e., ET, HT, and CT) could also be problematic. However the exact reason for the insufficiency of the analysis is unclear.

As found from previous theoretical studies, the key factor for crystallochromy is the value of electronic coupling. Therefore, an accurate description of electronic coupling is required for clarifying the underlying mechanism. One of the authors (K.J.F.) previously developed the transition-density-fragment interaction combined with transfer integral (TDFI-TI) method for EET via CT states.<sup>22</sup> The TDFI-TI method describes electronic couplings in terms of five contributions (i.e., Coulomb, exchange, ET, HT, and CT interactions), which succeeded in quantitatively reproducing the reference values of electronic couplings when applied to an ethylene dimer.<sup>22</sup> Taking into account the similarity on electronic couplings between EET and crystallochromy, the TDFI-TI method is expected to be applicable to crystallochromy.

This study attempts to account for the mechanism of crystallochromy on the red and yellow solids of tetracenes, such as BUR and BUY. For this purpose, we first perform absorption and fluorescence energy calculations using the TDFI-TI method, and next the calculated values are compared with experimental ones. Based on our successful description of the experimental spectra, the underlying molecular mechanism is explored.

## II. THEORY

As mentioned in the Introduction, the key factor for crystallochromy is to obtain accurate values of electronic couplings. In this section, we briefly explain the calculation

schemes of electronic couplings and absorption spectra. The details of the TDFI-TI method are described in Ref. 22.

### A. Electronic coupling calculations

The total Hamiltonian for  $N$  molecules is given by

$$\hat{H} = \sum_i^N \hat{H}_i + \sum_i^N \sum_{j>i}^N \hat{V}_{ij}, \quad (1)$$

where  $\hat{H}_i$  is the local Hamiltonian for the molecule  $i$  and  $\hat{V}_{ij}$  is the Coulomb interactions between the different molecules  $i$  and  $j$ . Using Eq. (1), the Hamiltonian matrix is constructed. The basic structure of the Hamiltonian matrix is written as<sup>23,24</sup>

$$\mathbf{H} = \begin{pmatrix} \mathbf{H}_{\text{LE}} & \mathbf{H}_{\text{LE-CT}} \\ \mathbf{H}_{\text{CT-LE}} & \mathbf{H}_{\text{CT}} \end{pmatrix}, \quad (2)$$

where  $\mathbf{H}_{\text{LE}}$  and  $\mathbf{H}_{\text{CT}}$  are the block matrices for the LE and CT states, respectively, and  $\mathbf{H}_{\text{LE-CT}}$  and  $\mathbf{H}_{\text{CT-LE}}$  are the mixing blocks between the LE and CT states.

For simplicity, let us consider only four states for the molecules  $i$  and  $j$  (i.e.,  $N = 2$ ). The basis functions are given by

$$\begin{aligned} |\Phi_1\rangle &= |\psi_i^e \cdot \psi_j^g\rangle, \\ |\Phi_2\rangle &= |\psi_i^g \cdot \psi_j^e\rangle, \\ |\Phi_3\rangle &= |\psi_i^+ \cdot \psi_j^-\rangle, \\ |\Phi_4\rangle &= |\psi_i^- \cdot \psi_j^+\rangle, \end{aligned} \quad (3)$$

where  $\psi_x^g$  and  $\psi_x^e$  represent the ground ( $g$ ) and excited ( $e$ ) states for the molecule  $x$  ( $x = i$  or  $j$ ), respectively, and  $\psi_x^+$  and  $\psi_x^-$  are the cationic and anionic states for the molecule  $x$ , respectively. Using these basis functions, the  $4 \times 4$  Hamiltonian matrix is described as

$$\mathbf{H} = \begin{pmatrix} E_1 & V_{\text{EET}} & V_{\text{ET}} & V_{\text{HT}} \\ V_{\text{EET}} & E_2 & V_{\text{HT}} & V_{\text{ET}} \\ V_{\text{ET}} & V_{\text{HT}} & E_3 & V_{\text{CT}} \\ V_{\text{HT}} & V_{\text{ET}} & V_{\text{CT}} & E_4 \end{pmatrix}. \quad (4)$$

In Eq. (4), the first and second diagonal elements,  $E_1$  and  $E_2$ , correspond to the  $\mathbf{H}_{\text{LE}}$  block in Eq. (2). These elements are calculated with the density-fragment interaction (DFI) method:<sup>22,25–27</sup>

$$\begin{aligned} E_1 &= E_{\text{ex}}^i + \sum_{v,\mu \in i} (P_{v\mu}^{ie} - P_{v\mu}^{ig}) \\ &\times \left\{ v_{\mu v}^j + \sum_{\lambda, \sigma \in j} P_{\lambda\sigma}^{jg} \left[ (\mu v | \sigma \lambda) - \frac{1}{2} (\mu \lambda | \sigma v) \right] \right\}, \quad (5a) \end{aligned}$$

$$\begin{aligned} E_2 &= E_{\text{ex}}^j + \sum_{v,\mu \in j} (P_{v\mu}^{je} - P_{v\mu}^{jg}) \\ &\times \left\{ v_{\mu v}^i + \sum_{\lambda, \sigma \in i} P_{\lambda\sigma}^{ig} \left[ (\mu v | \sigma \lambda) - \frac{1}{2} (\mu \lambda | \sigma v) \right] \right\}, \quad (5b) \end{aligned}$$



where  $E_{\text{ex}}^x$  is the excitation energy of the monomer  $x$ ,  $P_{\nu\mu}^{xs}$  is the 1-electron density matrix for the state  $s$  ( $s = g$  or  $e$ ) of the monomer  $x$ ,  $v_{\mu\nu}^x$  is the nuclear potential matrix generated from the counterpart molecule  $x$ , and  $(\mu\nu|\sigma\lambda)$  is the atomic orbital (AO) two-electron integral defined by  $(\mu\nu|\sigma\lambda) \equiv \int d\mathbf{r}_1 \int d\mathbf{r}_2 \chi_{\mu}^*(\mathbf{r}_1) \chi_{\nu}(\mathbf{r}_1) r_{12}^{-1} \chi_{\sigma}^*(\mathbf{r}_2) \chi_{\lambda}(\mathbf{r}_2)$ . We note that Eqs. (5a) and (5b) correspond to the excitation energies that include the electronic polarization effect induced by the Coulomb and exchange interactions with the counterpart molecule.<sup>22,27</sup>

The third and fourth diagonal elements,  $E_3$  and  $E_4$ , represent the energies for the charge separated states, and they correspond to the  $\mathbf{H}_{\text{CT}}$  block in Eq. (2). Here, we consider the charge separated states related only to the highest occupied molecular orbital (HOMO) and lowest unoccupied molecular orbital (LUMO) for simplicity. According to Koopmans' theorem,<sup>28</sup> the energies are expressed as

$$E_3 = -\varepsilon_{\text{H}}^i - \varepsilon_{\text{L}}^j - \sum_{\mu, \nu \in i} \sum_{\lambda, \sigma \in j} c_{\nu\text{H}}^i c_{\text{H}\mu}^i c_{\lambda\text{L}}^j c_{\text{L}\sigma}^j (\mu\nu|\sigma\lambda), \quad (6a)$$

$$E_4 = \varepsilon_{\text{L}}^i - \varepsilon_{\text{H}}^j - \sum_{\mu, \nu \in i} \sum_{\lambda, \sigma \in j} c_{\nu\text{L}}^i c_{\text{L}\mu}^i c_{\lambda\text{H}}^j c_{\text{H}\sigma}^j (\mu\nu|\sigma\lambda), \quad (6b)$$

where  $\varepsilon_{\text{H}}^x$  and  $\varepsilon_{\text{L}}^x$  denote the orbital energies for HOMO and LUMO of the molecule  $x$ , respectively, and  $c_{\nu\text{H}}^x$  and  $c_{\lambda\text{L}}^x$  are their linear combination of AO-MO (LCAO-MO) coefficients. The third terms in Eqs. (6a) and (6b) represent the HOMO-LUMO interaction between the two molecules.

The four off-diagonal elements in Eq. (4) are written as follows:<sup>22</sup>

$$V_{\text{EET}} = \sum_{\nu, \mu \in i} \sum_{\lambda, \sigma \in j} P_{\nu\mu}^{ieg} P_{\lambda\sigma}^{jeg} \left[ (\mu\nu|\sigma\lambda) - \frac{1}{2}(\mu\lambda|\sigma\nu) \right] \\ \equiv V_{\text{Coul}} + V_{\text{Exch}}, \quad (7a)$$

$$V_{\text{ET}} = t_{\text{H} \rightarrow \text{L}}^i \left\{ \sum_{\alpha \in i} \sum_{\beta \in j} c_{\text{L}\alpha}^i F_{\alpha\beta} c_{\beta\text{L}}^j + \sum_{\mu \in i} \sum_{\nu \in i} c_{\nu\text{H}}^i c_{\text{L}\mu}^i \right. \\ \left. \times \sum_{\sigma \in i} \sum_{\lambda \in j} c_{\lambda\text{L}}^j c_{\text{H}\sigma}^i [2(\mu\nu|\sigma\lambda) - (\mu\lambda|\sigma\nu)] \right\}, \quad (7b)$$

$$V_{\text{HT}} = t_{\text{H} \rightarrow \text{L}}^i \left\{ - \sum_{\alpha \in i} \sum_{\beta \in j} c_{\text{H}\alpha}^i F_{\alpha\beta} c_{\beta\text{H}}^j + \sum_{\mu \in i} \sum_{\nu \in i} c_{\nu\text{L}}^i c_{\text{H}\mu}^i \right. \\ \left. \times \sum_{\sigma \in i} \sum_{\lambda \in j} c_{\lambda\text{H}}^j c_{\text{L}\sigma}^i [2(\mu\nu|\sigma\lambda) - (\mu\lambda|\sigma\nu)] \right\}, \quad (7c)$$

$$V_{\text{CT}} = \sum_{\mu \in i} \sum_{\nu \in j} c_{\nu\text{L}}^j c_{\text{H}\mu}^i \sum_{\sigma \in i} \sum_{\lambda \in j} c_{\lambda\text{H}}^j c_{\text{L}\sigma}^i [2(\mu\nu|\sigma\lambda) - (\mu\lambda|\sigma\nu)], \quad (7d)$$

where  $P_{\nu\mu}^{xeg}$  is the 1-electron transition density matrix for the monomer  $x$ ,  $F_{\alpha\beta}$  is the Fock matrix, and  $t_{\text{H} \rightarrow \text{L}}^x$  is the configuration interaction (CI) coefficient of the HOMO-LUMO transition. The first and second terms of  $V_{\text{EET}}$  correspond to elec-

tronic couplings of the Coulomb ( $V_{\text{Coul}}$ ) and exchange ( $V_{\text{Exch}}$ ) interactions between two molecules, which can be calculated with the TDFI method.<sup>22,26,27</sup> On the other hand,  $V_{\text{ET}}$ ,  $V_{\text{HT}}$ , and  $V_{\text{CT}}$  express electronic couplings of the ET, HT, and CT interactions, respectively, which can be calculated with the TI method.<sup>17,29</sup> Here, we note that Eqs. (7b)–(7d) represent the intermolecular interactions related only to HOMOs or LUMOs of two molecules. In the cases of the other orbital interactions, the appropriate expressions can be obtained by replacing the LCAO-MO coefficients in Eqs. (7b)–(7d) by the corresponding ones.

The  $K$ th excited state for the total system is expressed by a linear combination of Eq. (3) (in this case,  $l = 1$  to 4):

$$|\Psi_K\rangle = \sum_l C_{lK} |\Phi_l\rangle. \quad (8)$$

To determine the expansion coefficients  $C_{lK}$ , we need to diagonalize the Hamiltonian matrix  $\mathbf{H}$ . However, the standard diagonalization procedure is not applicable to  $\mathbf{H}$  because the basis functions  $|\Phi_l\rangle$  are not orthogonal. To overcome this problem, we employed the Löwdin symmetric orthogonalization method<sup>30</sup> which transforms  $\mathbf{H}$  to the orthogonal representation:

$$\mathbf{S}^{-1/2} \mathbf{H} \mathbf{S}^{-1/2} = \mathbf{H}_s, \quad (9)$$

where  $\mathbf{H}_s$  is the Hamiltonian matrix in the symmetrically orthogonal representation and  $\mathbf{S}^{-1/2}$  represents the transformation matrix.  $\mathbf{S}$  is the overlap matrix of the basis functions, defined by  $S_{kl} \equiv \langle \Phi_k | \Phi_l \rangle$ . Owing to this treatment, the matrix  $\mathbf{H}_s$  can be diagonalized:

$$\mathbf{U}^\dagger \mathbf{H}_s \mathbf{U} = \mathbf{H}_d. \quad (10)$$

Following this procedure, the state energies  $E_K$  and the expansion coefficients  $C_{lK}$  are obtained from the diagonal elements of  $\mathbf{H}_d$  and from the elements of the transformation matrix  $\mathbf{X}$  ( $\mathbf{X} = \mathbf{S}^{-1/2} \mathbf{U}$ ), respectively. Since the ground state energy is set to be zero in this scheme,  $E_K$  directly corresponds to the excitation energies for the interacting systems. Combining the matrix  $\mathbf{X}$  with the non-interacting electric transition dipole moments  $\mathbf{d}_l^{eg}$ , we can obtain the transition dipole moments for the interacting system as<sup>27</sup>

$$\mathbf{D}_K^{eg} = \sum_l X_{lK} \mathbf{d}_l^{eg}. \quad (11)$$

Using this transition dipole, the oscillator strength  $f_K$  is calculated

$$f_K = \frac{2}{3} E_K |\mathbf{D}_K^{eg}|^2. \quad (12)$$

## B. Absorption spectrum calculations

Intensity distribution in the absorption spectra is approximated with Gaussian functions

$$I(E) = \sum_K \frac{f_K}{\sqrt{2\pi k_B T S}} \exp \left[ -\frac{(E - E_K)^2}{2k_B T S} \right], \quad (13)$$

where  $k_B$ ,  $T$ , and  $S$  denote Boltzmann constant, temperature, and Stokes shift, respectively. In this study, we also



consider the vibrational progression. In such a case, the intensity spectrum is expressed with the Franck-Condon factor and Lorentzian functions.<sup>31</sup>

$$I(E) = \sum_K \sum_{n=0,1,2,\dots} \exp(-s_{\text{HR}}) \frac{s_{\text{HR}}^n}{n!} \frac{f_K}{\pi} \times \frac{\gamma}{(E - E_K - n\hbar\omega_{\text{eff}})^2 + \gamma^2}. \quad (14)$$

The linewidth is given by

$$\gamma = \frac{k_B T S}{\hbar\omega_{\text{eff}}}, \quad (15)$$

where  $\hbar$  is Planck's constant divided by  $2\pi$ , and  $\omega_{\text{eff}}$  is the effective vibrational angular frequency. This value is calculated by<sup>32</sup>

$$\omega_{\text{eff}} = \sqrt{\frac{\sum_m \omega_m^2 \lambda_m}{\sum_m \lambda_m}}, \quad (16)$$

where  $\omega_m$  and  $\lambda_m$  are the vibrational angular frequency and the reorganization energy for the normal mode  $m$ , respectively. Using this frequency, the effective Huang-Rhys (HR) factor  $s_{\text{HR}}$ <sup>33,34</sup> is obtained:

$$s_{\text{HR}} = \frac{\sum_m \lambda_m}{\hbar\omega_{\text{eff}}}. \quad (17)$$

### III. COMPUTATIONAL DETAILS

The atomic coordinates of BUR and BUY were obtained from the crystallographic structures<sup>21</sup> (Cambridge Crystallographic Data Center code: CCDC-642337 for BUR and CCDC-642338 for BUY). These structures were optimized with the multicore quantum mechanics and molecular mechanics (mcQM/MM) method,<sup>35</sup> in which 11232 atoms (144 molecules) were taken into account as total systems. In the mcQM/MM optimizations, a single molecule was treated as the QM region, while the rest parts were as the MM one. In the ground state calculations, the QM atoms were described with density functional theory (DFT)<sup>36</sup> using the B3LYP functional,<sup>37</sup> in which the split valence double- $\zeta$  plus polarization basis set (6-31G\*) was used. In the excited state calculations, we employed time-dependent DFT (TD-DFT)<sup>38</sup> at the B3LYP/6-31G\* level. For the MM atoms, the general amber force field (GAFF)<sup>39</sup> was employed. The optimized structures of BUR and BUY are shown in Figs. 1(a) and 1(b), and these structures were used for the TDFI-TI calculations.

The CI-singles (CIS),<sup>40</sup> TD-DFT, and symmetry-adapted cluster-CI (SAC-CI)<sup>41</sup> methods with a frozen core approximation to 1s core orbitals were employed for obtaining the excitation energies and the transition densities. In the TD-DFT calculations, the revised Coulomb-attenuating method (rCAM) B3LYP functional<sup>42</sup> was used. The electrostatic solid-state effect was described with the MM atoms, and the molecular orbitals polarized by the MM atoms were used for the absorption and fluorescence energy calculations. The solvent effect of *n*-hexane was included with the polarized continuum model (PCM),<sup>43</sup> in which the dielectric constant and

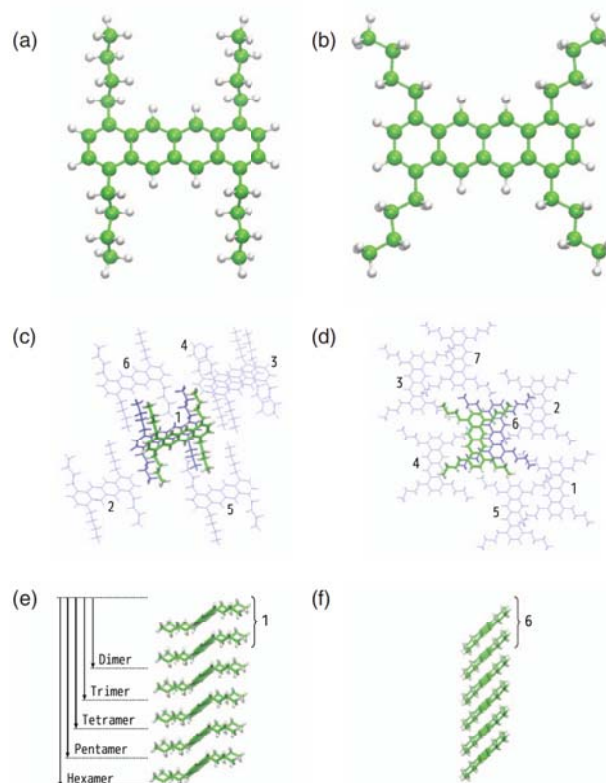


FIG. 1. Molecular structures of BUR and BUY. (a) BUR monomer, (b) BUY monomer, (c) dimer conformations in BUR crystal, (d) dimer conformations in BUY crystal, (e) BUR hexamer, (f) BUY hexamer. In (c) and (d), the central molecules and the selected molecules are colored green and blue, respectively. Each dimer conformation is numbered as 1 to 6 in (c) and as 1 to 7 in (d). The numbers in (e) and (f) correspond to the dimer conformations 1 and 6 for BUR and BUY, respectively.

the dielectric constant at infinite frequency were set to the default values ( $\epsilon = 1.88190$  and  $\epsilon_{\infty} = 1.89035$ ).

In the TDFI-TI calculations, the DFI algorithm<sup>25</sup> was used to satisfy the self-consistency condition between interacting molecules. Owing to this treatment, the inter-fragment polarization effect was included in the electron densities in Eqs. (5a) and (5b), the transition densities in Eq. (7a), and the LCAO-MO coefficients in Eqs. (7b)–(7d). To describe the multimerization effects, we considered not only the HOMOs and LUMOs but also the HOMO + 1s and LUMO + 1s as the cationic and anionic states of the basis functions (e.g.,  $|\psi_i^{H-1} \cdot \psi_j^L\rangle$ ,  $|\psi_i^{H-1} \cdot \psi_j^{L+1}\rangle$ ,  $|\psi_i^H \cdot \psi_j^L\rangle$ ,  $|\psi_i^H \cdot \psi_j^{L+1}\rangle$ ,  $|\psi_i^L \cdot \psi_j^{H-1}\rangle$ ,  $|\psi_i^L \cdot \psi_j^H\rangle$ ,  $|\psi_i^{L+1} \cdot \psi_j^{H-1}\rangle$ , and  $|\psi_i^{L+1} \cdot \psi_j^H\rangle$  for dimer), and hence the pair of the cationic and anionic states was selected from adjacent molecules (e.g.,  $|\psi_i^{H-1} \cdot \psi_j^L \cdot \psi_k^g\rangle$ ,  $|\psi_i^{H-1} \cdot \psi_j^{L+1} \cdot \psi_k^g\rangle$ ,  $|\psi_i^H \cdot \psi_j^L \cdot \psi_k^g\rangle$ ,  $|\psi_i^H \cdot \psi_j^{L+1} \cdot \psi_k^g\rangle$ ,  $|\psi_i^L \cdot \psi_j^{H-1} \cdot \psi_k^g\rangle$ ,  $|\psi_i^L \cdot \psi_j^H \cdot \psi_k^g\rangle$ ,  $|\psi_i^{L+1} \cdot \psi_j^{H-1} \cdot \psi_k^g\rangle$ ,  $|\psi_i^{L+1} \cdot \psi_j^H \cdot \psi_k^g\rangle$ ,  $|\psi_i^g \cdot \psi_j^{H-1} \cdot \psi_k^L\rangle$ ,  $|\psi_i^g \cdot \psi_j^H \cdot \psi_k^L\rangle$ ,  $|\psi_i^g \cdot \psi_j^{L+1} \cdot \psi_k^L\rangle$ ,  $|\psi_i^g \cdot \psi_j^L \cdot \psi_k^{H-1}\rangle$ ,  $|\psi_i^g \cdot \psi_j^L \cdot \psi_k^H\rangle$ ,  $|\psi_i^g \cdot \psi_j^{L+1} \cdot \psi_k^{H-1}\rangle$ , and  $|\psi_i^g \cdot \psi_j^{L+1} \cdot \psi_k^H\rangle$  for trimer). In the case of  $N$ -mer, the  $(9N - 8) \times (9N - 8)$  Hamiltonian matrix was, therefore, computed.



To obtain the spectral linewidth, the vibrational analysis at the B3LYP/6-31G\* level was performed to the optimized geometry. Here, the scaling factor of 0.9613 was applied.<sup>44</sup> From this analysis, the normal mode coordinates and frequencies were obtained, which were used for calculating the effective angular frequency and HR factor. Temperature for the intensity distribution was set to be  $T = 300$  K, and the value of Stokes shift was calculated from the difference between absorption and fluorescence energies.

The mcQM/MM computations were carried out with TINKER4.2<sup>45</sup> interfaced with the GAUSSIAN03 program package.<sup>46</sup> The vibrational analysis was performed with GAUSSIAN03. The TDFI-TI program with CIS, TD-DFT, and SAC-CI were implemented in GAUSSIAN03.

## IV. RESULTS AND DISCUSSION

### A. Effect of the alkyl side-chain conformation on the absorption energy

As shown in Figs. 1(a) and 1(b), the optimized structures of BUR and BUY are different in the conformation of the alkyl side-chain. The side chains in BUR have in-plane conformations, while those in BUY are out-of-plane ones. To check the conformational effect on the absorption energy, we calculated the gas-phase absorption energies of BUR and BUY, for which the monomer structures isolated from the mcQM/MM optimized ones were used. As listed in Table I, the absorption energies obtained with the SAC-CI method were to be 2.56 eV and 2.68 eV for BUR and BUY, respectively. These absorption energies were obtained from the first excited states, and their characters were to be the  $\pi$ - $\pi^*$  excitations (the HOMO-LUMO transitions). From the comparison of these values, the difference in the absorption energies between BUR and BUY was evaluated to be 0.12 eV. The similar spectral shifts can be seen in the CIS (0.11 eV) and TD-rCAM-B3LYP (0.10 eV) results, although the absolute absorption energies depend on the electronic structure methods employed.

We also performed the absorption energy calculations in solid state, which were compared between BUR and BUY. Here, the solid environment surrounding the single molecule (BUR or BUY) was approximated with the MM atoms. The results are also listed in Table I. The SAC-CI absorption energies became 2.56 eV and 2.67 eV for BUR and BUY, respectively. Compared with the gas-phase absorption energies (2.56 eV for BUR and 2.68 eV for BUY), the electrostatic solid-state effect was estimated to be 0.00 eV and  $-0.01$  eV

for BUR and BUY, respectively. In addition, the spectral shift between BUR and BUY was to be 0.11 eV. The CIS and TD-rCAM-B3LYP methods provided the similar spectral shift to the SAC-CI one (0.11 eV for CIS and 0.10 eV for TD-rCAM-B3LYP). By comparing the spectral shift in solid state with that in gas phase, the contributions from the electrostatic solid-state effects were estimated to be  $-0.01$  eV, 0.00 eV, and 0.00 eV for SAC-CI, CIS, and TD-rCAM-B3LYP, respectively.

From these results, the side-chain conformational effect was found to give a non-negligible contribution to the spectral shift between BUR and BUY ( $\sim 0.12$  eV), while the solid-state effect approximated with the MM atoms was to be very small ( $\sim -0.01$  eV). In spite of the large contribution from the side-chain conformational effect, these calculations could not reproduce the experimentally observed spectral shift between BUR and BUY (0.38 eV<sup>21</sup>). The deviations of 0.27–0.28 eV from the experimental values remained yet. Therefore, the consideration of only the side-chain conformational effect was found to be insufficient for explaining the experimental spectral shift between BUR and BUY.

In addition, the absolute absorption energies calculated were confirmed to strongly depend on the electronic structure methods (2.56–3.44 eV for BUR and 2.67–3.55 eV for BUY). The closest values to the experimental ones (2.18 eV for BUR and 2.56 eV for BUY) were obtained from the SAC-CI results. Since these calculations took into account only the single molecule (i.e., the monomer BUR or BUY) as the QM atoms, we could not simply compare the calculated values with the experimental solid-state absorption energies. To further investigate the dependence on the electronic structure methods, we calculated the absorption energies in solution, and compared them with the experimental value. Since the molecular structure in solution was not observed in experiments, the crystallographic structures of BUR and BUY were employed. These structures were optimized with the B3LYP/6-31G\* method. In both the geometry optimization and the absorption energy calculation, the solvent effect was included with the PCM method. The calculated absorption energies are also listed in Table I. In the BUR calculations, the SAC-CI, CIS, and TD-rCAM-B3LYP methods provided the absorption energies of 2.51 eV, 3.28 eV, and 3.07 eV, respectively. In the case of BUY, the SAC-CI, CIS, and TD-rCAM-B3LYP results were to be 2.63 eV, 3.38 eV, and 3.17 eV, respectively. Therefore, the SAC-CI method was found to better reproduce the experimental value (2.57 eV<sup>21</sup>). The deviation from the experimental value was to be  $-0.06$  eV in the case of BUR and 0.06 eV for BUY. Based on these results, the

TABLE I. Calculated absorption energies of the BUR and BUY monomers (eV).

|               | In vacuo |      | In crystal |                    |      |                    | In <i>n</i> -hexane |                  |                    |
|---------------|----------|------|------------|--------------------|------|--------------------|---------------------|------------------|--------------------|
|               | BUR      | BUY  | BUR        | Expt. <sup>a</sup> | BUY  | Expt. <sup>a</sup> | BUR <sup>b</sup>    | BUY <sup>b</sup> | Expt. <sup>a</sup> |
| SAC-CI        | 2.56     | 2.68 | 2.56       |                    | 2.67 |                    | 2.51                | 2.63             |                    |
| TD-rCAM-B3LYP | 3.12     | 3.22 | 3.11       | 2.18               | 3.21 | 2.56               | 3.07                | 3.17             | 2.57               |
| CIS           | 3.44     | 3.55 | 3.44       |                    | 3.55 |                    | 3.28                | 3.38             |                    |

<sup>a</sup>Experimental data described in Ref. 21.

<sup>b</sup>Optimized structure with the PCM method was used.



TABLE II. TDFI-TI absorption energies of the BUR and BUY dimers (eV).<sup>a</sup>

|     | 1 <sup>b</sup> | 2 <sup>b</sup> | 3 <sup>b</sup> | 4 <sup>b</sup> | 5 <sup>b</sup> | 6 <sup>b</sup> | 7 <sup>b</sup> |
|-----|----------------|----------------|----------------|----------------|----------------|----------------|----------------|
| BUR | 2.37           | 2.55           | 2.56           | 2.55           | 2.56           | 2.56           | ...            |
| BUY | 2.68           | 2.68           | 2.68           | 2.68           | 2.68           | 2.65           | 2.68           |

<sup>a</sup>SAC-CI data are employed.<sup>b</sup>The number corresponds to the dimer conformation shown in Figs. 1(c) and 1(d).

SAC-CI method was mainly employed in Secs. IV B–IV D. The SAC-CI results seemed to indicate that the molecular structure in solution is composed of the mixture of BUR and BUY. However, the present study does not focus on this topic.

## B. The multimerization effect and the electrostatic solid-state effect

To investigate the dependence on the molecular arrangement, the absorption energy calculations were performed to several dimer conformations. Figures 1(c) and 1(d) show the molecular conformations employed in the dimer calculations. Each dimer conformation was extracted from the mcQM/MM geometries of BUR and BUY. For the molecular selection, we used the shortest atom-to-atom distance between the pair of molecules. The distance was measured from a central molecule colored green in Figs. 1(c) and 1(d). If the distance was within 3.0 Å, the molecule was selected. Hence, only half of the selected molecules were employed for the dimer calculations because of the spatial symmetry. In Figs. 1(c) and 1(d), the selected molecules are colored blue and numbered as 1 to 6 for BUR and as 1 to 7 for BUY. The results of the absorption energies are summarized in Table II. Here, we note that the absorption energies were calculated with the procedure of Sec. II A. In BUR, the absorption energies calculated with the individual dimer conformations ranged between 2.37 eV and 2.56 eV, and the smallest value (2.37 eV) was obtained from the dimer conformation 1. Subtracting the gas-phase absorption energy of the monomer BUR (2.56 eV) from the smallest value, the dimerization effect was estimated to be −0.19 eV. On the other hand, the calculated absorption energies for the BUY dimers were in between 2.65 eV and 2.68 eV, and the smallest value (2.65 eV) was obtained from the dimer conformation 6. Therefore, the dimerization effect was estimated to be −0.03 eV from the comparison with the monomer absorption energy of BUY (2.68 eV). From these results, the dimer conformations 1 for BUR and 6 for BUY were found to have the most red-shifted absorption energies among all the cal-

culated dimers. In other words, the rest of the dimer conformations exhibited a few changes in the absorption energies, compared with the monomer cases (~0.01 eV for BUR and ~0.00 eV for BUY).

We next examined the dependence of the absorption energy on the number of molecules. To this end, the absorption energy calculations were performed to the trimer-hexamer conformations. As mentioned above, the dimer conformations 1 for BUR and 6 for BUY largely contributed to the spectral shifts. As shown in Figs. 1(c) and 1(d), these dimers were confirmed to have stacked conformations while the other conformations were not stacked. Therefore, we here focused on the dimer conformations 1 for BUR and 6 for BUY as reference structures of the individual multimers. The molecular structures used in the calculations are shown in Figs. 1(e) and 1(f). As found here, both the multimers are constructed so as to elongate the reference structure in the direction of the center-to-center separation between two molecules. Each multimer conformation was extracted from the mcQM/MM geometries of BUR and BUY. The results of the absorption energies are summarized in Table III. The calculated values of BUR were to be 2.29 eV, 2.25 eV, 2.23 eV, and 2.23 eV for the trimer, tetramer, pentamer, and hexamer, respectively, while those of BUY were to be 2.62 eV, 2.61 eV, 2.61 eV, and 2.61 eV in the same order. Therefore, the energy convergence less than 0.01 eV could be satisfied by the hexamer calculations. Based on these results, we attempted to evaluate the contribution from the multimerization effect to the spectral shift. First, the amount of the spectral shift was calculated to be 0.38 eV from the comparison of the absorption energies between BUR (2.23 eV) and BUY (2.61 eV). Next, the multimerization effects were calculated to be −0.33 eV and −0.07 eV for BUR and BUY, respectively, by subtracting the monomer absorption energies from the hexamer ones. Therefore, the difference in the multimerization effects was estimated to be 0.26 eV. From these results, the multimerization effect was found to contribute 68.4% to the spectral shift between BUR and BUY. We further compared the contribution from the dimerization effect with that from the multimerization effect. The contribution from the dimerization effect to the spectral shift was calculated to be 0.16 eV by comparing the dimerization effects between BUR (−0.19 eV) and BUY (−0.03 eV), and thus it became 61.5% of the multimerization effect. From these results, the dimerization effect was found to mainly contribute to the multimerization effect.

The above calculations were based only on the multimer conformations shown in Figs. 1(e) and 1(f). This was because the dimer conformations 1 for BUR and 6 for BUY largely

TABLE III. TDFI-TI absorption energies of the BUR and BUY *N*-mers (eV).<sup>a</sup>

|     | Monomer | Dimer                     | Trimer | Tetramer | Pentamer | Hexamer                                       |
|-----|---------|---------------------------|--------|----------|----------|---|
| BUR | 2.56    | 2.37 (2.55 <sup>b</sup> ) | 2.29   | 2.25     | 2.23     | 2.23 (2.23 <sup>c</sup> , 1.90 <sup>d</sup> ) |
| BUY | 2.68    | 2.65 (2.67 <sup>b</sup> ) | 2.62   | 2.61     | 2.61     | 2.61 (2.62 <sup>c</sup> , 2.20 <sup>d</sup> ) |

<sup>a</sup>SAC-CI data are employed.<sup>b</sup>2-state model result.<sup>c</sup>Absorption energy calculated in crystal.<sup>d</sup>Fluorescence energy calculated in crystal.



contributed to the spectral shifts. We also focused on the other multimer conformations and evaluated the multimerization effects. These evaluations were performed on the basis of the dimer conformations shown in Figs. 1(c) and 1(d) (i.e., the dimer conformations 2-6 for BUR, and 1-5 and 7 for BUY). Similar to Figs. 1(e) and 1(f), the linearly elongated dimer conformations were used for the multimer calculations. As a result, the calculated absorption energies were to be 2.54–2.56 eV for BUR and 2.66–2.68 eV for BUY. The energy convergence less than 0.01 eV was satisfied by the trimer calculations for all the multimer conformations calculated. As found from these results, the calculated absorption energies were almost the same as the monomer ones. The multimerization effects brought about the spectral red-shift of only  $\sim 0.02$  eV and  $\sim 0.02$  eV for BUR and BUY, respectively. From these results, we confirmed that the spectral shifts of BUR and BUY were predominantly caused by the multimer conformations shown in Figs. 1(e) and 1(f) and that the other conformations provided a few contributions to the spectral shifts.

Similar to the monomer case, we performed the absorption energy calculations in solid state, using the hexamer conformations of BUR and BUY. Here again, the solid environment was described with the MM atoms. As also listed in Table III, the solid-state absorption energies for BUR and BUY were to be 2.23 eV and 2.62 eV, respectively, so that the spectral shift between BUR and BUY was evaluated to be 0.39 eV. From the comparison with the gas-phase absorption energies (2.23 eV for BUR and 2.61 eV for BUY), the solid-state effects were estimated to be 0.00 eV and 0.01 eV for BUR and BUY, respectively. Hence, the contribution from the electrostatic solid-state effect to the spectral shift was estimated to be 0.01 eV by subtracting the spectral shift in gas phase (0.38 eV) from that in solid state (0.39 eV). Therefore, the electrostatic solid-state effect was confirmed to have a small contribution to the spectral shift also in the hexamer calculations.

As found from Table III, the absorption energies calculated with the hexamer conformations (Figs. 1(e) and 1(f)) successfully reproduced the experimental absorption energies<sup>21</sup> (2.18 eV for BUR and 2.56 eV for BUY). The deviations from the experimental values were to be 0.05 eV and 0.06 eV for BUR and BUY, respectively. Also on the spectral shift between BUR and BUY, the calculated value (0.39 eV) was well in agreement with the experimental one (0.38 eV) with the deviation of 0.01 eV. Comparing the three effects (i.e., the multimerization effect (0.26 eV), the side-chain conformational effect (0.12 eV), and the electrostatic solid-state effect (0.01 eV)), the multimerization effect was found to be the largest contribution to the spectral shift.

We also calculated the fluorescence energies using the hexamer conformations of BUR and BUY. In these calculations, the excited state geometries obtained with the mcQM/MM method were used, and the electrostatic solid-state effect was included with the MM atoms. As also listed in Table III, the calculated fluorescence energies were to be 1.90 eV and 2.20 eV for BUR and BUY, respectively, which were in agreement with the experimental values<sup>21</sup> (1.95 eV for BUR and 2.18 eV for BUY) with the deviations of 0.05 eV and 0.02 eV for BUR and BUY, respectively. The two fluores-

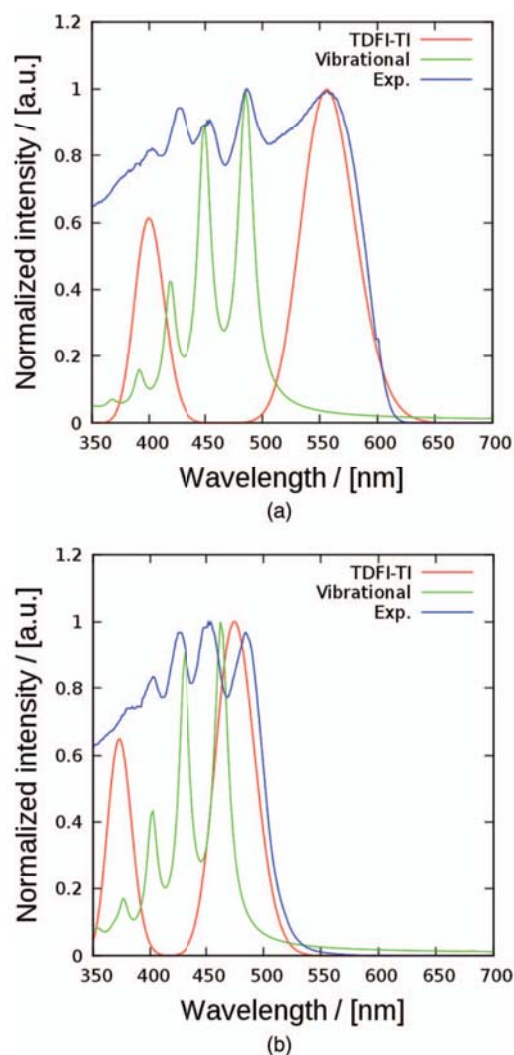


FIG. 2. Absorption spectra of (a) BUR and (b) BUY.

cence energies led to the spectral shift of 0.30 eV, which successfully reproduced the experimental spectral shift (0.23 eV) with the deviation of 0.07 eV.

### C. Solid-state spectra of BUR and BUY

Based on the successful reproductions of the experimental values, we calculated the absorption spectra for BUR and BUY, using two kinds of spectral shapes, Gaussian and Lorentzian functions. The spectral linewidth in Eq. (13) was calculated with  $T = 300$  K and  $S = 0.33$  eV, and the absorption energies obtained from the hexamer calculations were used for the spectral calculations. The results of the electronic spectra are shown by red lines in Fig. 2. As found here, these calculations successfully reproduced the first peaks in the experimental spectra of BUR and BUY. In particular, the red-shifted peak in the BUR spectrum was clearly represented by the calculation. As mentioned in Sec. IV B, the spectral shift was mainly caused by the difference in the multimerization effects between BUR and BUY. On the other hand, the rest of the experimental peaks could not be reproduced by these calculations. In the previous study, one of the authors (C.K.)



concluded that these peaks are attributed to the vibrational progressions.<sup>21</sup> Following this reason, we also calculated the vibrational spectra. These calculations were performed with the monomer absorption energies of BUR and BUY, and the spectral shapes were described with Eq. (14) where the effective angular frequency and HR factor obtained from the vibrational analysis were employed ( $\omega_{\text{eff}} = 1659 \text{ cm}^{-1}$  and  $s_{\text{HR}} = 0.874$ ). As shown by green lines in Fig. 2, these calculations well reproduced the positions of the second, third, and fourth peaks in the experimental spectra of BUR and BUY. Therefore, the influences of the vibrational progressions could be confirmed also from the calculated spectra.

#### D. Comparison of the EET interaction with the other interactions

As one of the useful features, the TDFI-TI method can describe electronic coupling in terms of five contributions (i.e., Coulomb, exchange, ET, HT, and CT interactions).<sup>22</sup> Using this advantage, we performed the absorption energy calculations based only on the LE basis functions (i.e.,  $\Phi_1$  and  $\Phi_2$  in Eq. (3)), where the Hamiltonian matrix expressed in Eq. (4) was reduced to the following form:

$$\mathbf{H} = \begin{pmatrix} E_1 & V_{\text{EET}} \\ V_{\text{EET}} & E_2 \end{pmatrix}. \quad (18)$$

Hereinafter, this is called as the 2-state model. The absorption energies calculated with the 2-state model were compared with the results from Secs. IV A and IV B. In these calculations, the dimer conformations 1 and 6 were used for BUR and BUY, respectively. As summarized in Table III, the absorption energies calculated with the 2-state model were to be 2.55 eV and 2.67 eV for BUR and BUY, respectively, which resulted in almost the same values as those obtained from the monomer calculations (2.56 eV for BUR and 2.68 eV for BUY). By comparing these values, the effects of the EET interaction (i.e., Coulomb and exchange) were estimated to be  $-0.01 \text{ eV}$  and  $-0.01 \text{ eV}$  for BUR and BUY, respectively. Therefore, both of the EET interactions were found to have small effects on the absorption energies. Since the EET interaction in Eq. (18) is one of electronic couplings and it is included in the dimerization effect mentioned in Sec. IV B ( $-0.19 \text{ eV}$  for BUR and  $-0.03 \text{ eV}$  for BUY), we compared the EET interaction effect with the dimerization effect. As a result, the EET interactions for BUR and BUY were found to cover 5.3% and 33.3% of the dimerization effects, respectively. From these results, the EET interaction in BUY was found to have a larger contribution to the dimerization effect than that in BUR.

As mentioned in the Introduction, the previous study attempted to explain the spectral shift between BUR and BUY with the molecular exciton model using the point dipole approximation.<sup>21</sup> However, those calculations failed in reproducing the experimental spectral shift. The spectral shift calculated in the previous study was to be  $0.16 \text{ eV}$ , which reproduced only 42.1% of the experimental value ( $0.38 \text{ eV}$ ). In those calculations, the EET interaction effects were estimated to be only  $-0.01 \text{ eV}$  and  $0.00 \text{ eV}$  for BUR and BUY, respectively. Based on these results, we consider two possibilities

of its cause. One is on the accuracy in the point dipole approximation for describing the EET interaction, and another is on the types of electronic couplings included in the absorption energy calculations. In the 2-state model calculations, we employed the TDFI method for calculating the EET interaction. As shown in the previous study,<sup>26,27</sup> TDFI can evaluate the EET interaction more accurately than the point dipole approximation. In spite of the high accuracy of TDFI, the 2-state model provided almost the same absorption energies as those obtained from the monomer calculations. Therefore, the EET interactions were found to have small effects ( $-0.01 \text{ eV}$ ) on the absorption energies. As shown in Sec. IV B, the inclusion of the multimerization effect led to the successful reproduction of the experimental absorption energy, and hence the dimerization effect was to be a main contribution to the multimerization effect. Since electronic couplings except for the EET interaction were also taken into account in the dimerization effect, the failure in the previous study was clarified to be attributed to the lack of the consideration of the ET, HT, and CT interactions, not to the accuracy in the point dipole approximation. Subtracting the EET interaction from the dimerization effect, the effects of electronic couplings except for the EET interaction were estimated to be  $-0.18 \text{ eV}$  and  $-0.02 \text{ eV}$  for BUR and BUY, respectively. Therefore, the contribution to the spectral shift between BUR and BUY was estimated to be  $0.16 \text{ eV}$ , which resulted in the same value as the contribution from the dimerization effect ( $0.16 \text{ eV}$ ). From these results, electronic coupling based on the ET, HT, and CT interactions was found to be the dominant factor for the spectral tuning between BUR and BUY.

#### E. Influence of the nodal character on the orbital energies

To further investigate the mechanism of the spectral tuning, we analyzed the MO pictures and the orbital energies. In the analysis, the dimer conformations 1 and 6 were used for BUR and BUY, respectively. Figure 3 illustrates the HOMO  $- 1s$ , HOMOs, LUMOs, and LUMO  $+ 1s$  for BUR and BUY. In BUR, the HOMO  $- 1$  and LUMO had the bonding characters and the HOMO and LUMO  $+ 1$  were to be the anti-bonding characters. As found from Figs. 3(a)–3(d), these orbital characters were easily distinguished. On the other hand, the characters of the four orbitals of BUY could not be identified due to the mixing of the bonding and anti-bonding characters. Regarding the orbital energy, the HOMO  $- 1$  and HOMO of BUR were to be  $-6.28 \text{ eV}$  and  $-5.81 \text{ eV}$ , respectively, which resulted in the orbital-energy gap of  $0.47 \text{ eV}$ . On the other hand, the HOMO  $- 1$  and HOMO of BUY were to be  $-6.20 \text{ eV}$  and  $-6.16 \text{ eV}$ , respectively, and the orbital-energy gap became  $0.04 \text{ eV}$ . Therefore, the HOMO  $- 1$ -HOMO gap of BUR was larger than that of BUY. The similar results were obtained from the LUMO-LUMO  $+ 1$  gap. The LUMO and LUMO  $+ 1$  of BUR were to be  $1.07 \text{ eV}$  and  $1.43 \text{ eV}$ , respectively, whereas those of BUY were to be  $1.20 \text{ eV}$  and  $1.31 \text{ eV}$ . Therefore, the LUMO-LUMO  $+ 1$  gap of BUR ( $0.36 \text{ eV}$ ) was larger than that of BUY ( $0.11 \text{ eV}$ ). On the HOMO-LUMO



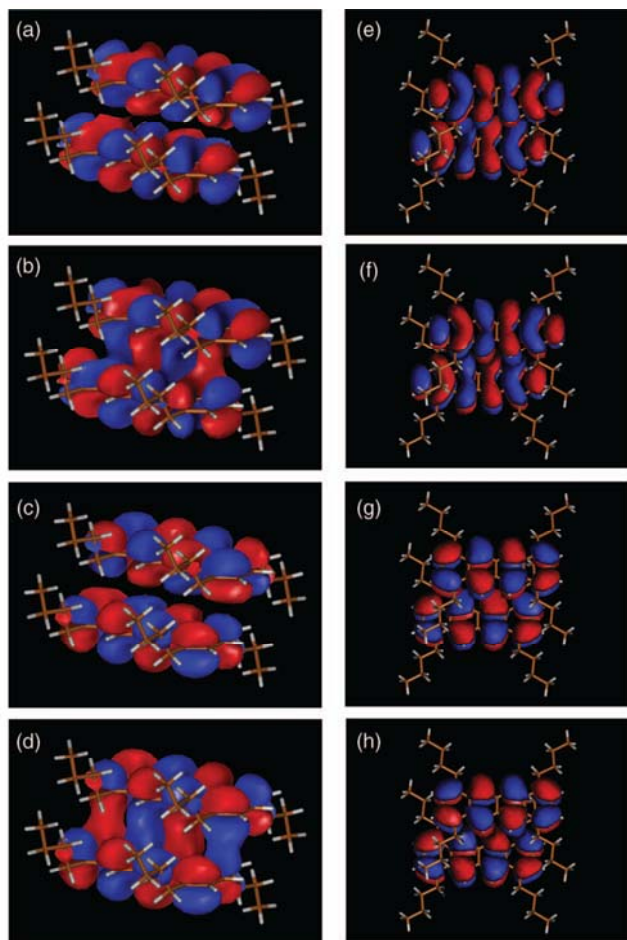


FIG. 3. (a) LUMO + 1, (b) LUMO, (c) HOMO, and (d) HOMO - 1 distributions of BUR dimer. (e) LUMO + 1, (f) LUMO, (g) HOMO, and (h) HOMO - 1 distributions of BUY dimer. The dimer conformations 1 for BUR and 6 for BUY are used.

gap, BUR had 6.88 eV, which was smaller by 0.48 eV than BUY (7.36 eV).

In general, when orbital characters are obviously identified, orbital interactions become strong. As a result, the orbital-energy gap is enlarged. Conversely, the mixing between the bonding and anti-bonding characters brings about the cancellation of the individual orbital interactions, which gives a few changes in the energy gap. In this way, the shift in the orbital energy is strongly related to the nodal characteristics of the molecular orbital. Based on this relationship, we could understand the difference in the orbital energies between BUR and BUY. In BUR, the clearly identified orbital characters gave rise to the strong orbital interactions, and thus HOMO - 1 and LUMO were stabilized and HOMO and LUMO + 1 were unstabilized. As a result, the HOMO - 1-HOMO gap and the LUMO-LUMO + 1 gap were to be large, while the HOMO-LUMO gap became small. In contrast, the mixing of the orbital characters in BUY caused a small change in the energy gap, because of the weak orbital interactions. Following these reasons, the HOMO-LUMO gap of BUR was smaller than that of BUY. As mentioned in Sec. IV B, the calculated absorption energy of BUR was red-shifted by 0.39 eV compared with that of BUY, so that the

difference in the HOMO-LUMO gap (0.48 eV) was found to qualitatively correspond to the calculated spectral shift.

In Sec. IV B, we showed that the BUR dimer 1 played a crucial role in the spectral red-shift. To understand the difference between the BUR dimer 1 and the others, the HOMO-LUMO gap calculations were performed also to the BUR dimers 2-6. As a result, the HOMO-LUMO gaps of the dimers 2-6 were calculated to be 7.24–7.31 eV. Comparing these values with the HOMO-LUMO gap of the BUR monomer (7.32 eV), the shifts in the HOMO-LUMO gap were to be 0.01–0.08 eV. In the case of the BUR dimer 1 (6.88 eV), the shift in the HOMO-LUMO gap was to be 0.44 eV. Therefore, the BUR dimer 1 was found to have a much larger contribution to the magnitude of the HOMO-LUMO gap than the other dimers. These results could be explained by the relationship between orbital characters and orbital interactions. As mentioned above, the clearly identified orbital characters for the dimer 1 made orbital interactions strong, which resulted in the small HOMO-LUMO gap. In contrast, molecular orbitals of the dimers 2-6 were similar to the monomer ones. In other words, the bonding and anti-bonding characters such as those observed in the BUR dimer 1 were not confirmed from the dimers 2-6. These results indicated the weak orbital interactions in the dimers 2-6, so that the shifts in the HOMO-LUMO gap became small. In this way, we could understand the difference in the HOMO-LUMO gaps between the BUR dimer 1 and the others. As mentioned in Sec. IV B, we found structural characteristics in BUR; only the BUR dimer 1 had a stacked conformation. This stacked conformation made the orbital characters different from those of the other conformations, which led to the small HOMO-LUMO gap and finally to the spectral red-shift.

As mentioned in Sec. IV D, electronic coupling based on the ET, HT, and CT interactions was larger in BUR than in BUY, which mainly contributed to the spectral tuning. This result could be understood from another perspective. In the Hückel method, the molecular orbitals of a homonuclear diatomic molecule, such as  $H_2$ , are obtained by solving the secular equation as<sup>47</sup>

$$\begin{vmatrix} \alpha - \varepsilon & \beta \\ \beta & \alpha - \varepsilon \end{vmatrix} = 0, \quad (19)$$

where  $\alpha$  and  $\beta$  are parameters represent Coulomb integral and resonance integral, respectively, and  $\varepsilon$  is the orbital energy. Since the orbital energies of Eq. (19) are calculated to be  $\alpha + \beta$  and  $\alpha - \beta$ , the size of energy splitting becomes  $2\beta$ . Therefore, the off-diagonal element,  $\beta$ , is to be important for orbital interaction. Similar to  $\beta$ , the value of electronic coupling corresponds to the off-diagonal element of the Hamiltonian matrix, as mentioned in Sec. II A. Hence, the size of energy splitting equals to twice of the electronic coupling if we consider a symmetric dimer with identical monomer energies. Therefore, electronic coupling is strongly related to orbital interaction. In fact, this relation is used in the so-called energy splitting in dimer (ESD) method<sup>29</sup> for calculating electronic coupling. Considering the relationship between orbital interaction and nodal characteristics, electronic coupling is related also to nodal characteristics. From these results, we



could understand that the spectral tuning between BUR and BUY originates from the difference in the orbital characters. This understanding was supported also by the difference in the HOMO-LUMO gap between BUR and BUY (0.48 eV).

### F. Relationship between the molecular displacement and the excited state characters

The influence of nodal characteristics on crystallochromy was first discussed by Kuzmaier and Hoffmann.<sup>16</sup> They performed the molecular orbital calculations to the various arrangements of the  $\pi$ -conjugated systems (ethylene, butadiene, and perylene), and clearly explained the dependence of the molecular-orbital bandwidth on the nodal characteristics. Following their study, we calculated the absorption energies of the tetracene dimer as a function of the intermolecular separation. The molecular displacement and the definition of the intermolecular separation are shown in Fig. 4. To reduce computational costs, we employed the TD-rCAM-B3LYP method imposing  $C_{2h}$  symmetry. The results of the absorption-energy curves are shown in Fig. 5(a). To examine the results, we also calculated the differences in the absorption energies between the first and second excited states, which are shown in Fig. 5(b). At 0.0 Å, the absorption energies of the first and second excited states were to be 2.51 eV and 3.20 eV, respectively, and thus the difference in the absorption energies became 0.69 eV. The energy difference decreased with increasing in the intermolecular distance, and it disappeared at 2.0 Å. In the region of 2.0–3.0 Å, the energy difference increased, and again it decreased at more than 3.0 Å. These results showed the dependence of the absorption energy on the intermolecular separation. To clarify the molecular mechanism, we analyzed the MO pictures and the orbital energies (data not shown). As a result, the clearly identified orbital characters were observed at 0.0 Å and 3.0 Å, whereas the characters at 2.0 Å were not identified due to the mixing of the bonding and anti-bonding characters. Similar to the results obtained in Sec. IV E, these orbital characters reflected the magnitude of the orbital-energy gap. The HOMO-LUMO gaps at 0.0 Å and 3.0 Å were smaller than that at 2.0 Å. Conversely, the HOMO – 1-LUMO gaps at 0.0 Å and 3.0 Å were larger than that at 2.0 Å. Therefore, the behaviors of the HOMO-LUMO gap and the HOMO – 1-LUMO gap qualitatively represented the absorption-energy curves for the first and second excited

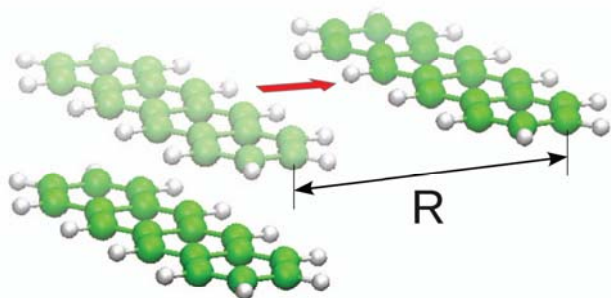


FIG. 4. Molecular displacement of tetracene dimer. The definition of  $x$ -axis coordinate for Figs. 5 and 6 is shown.

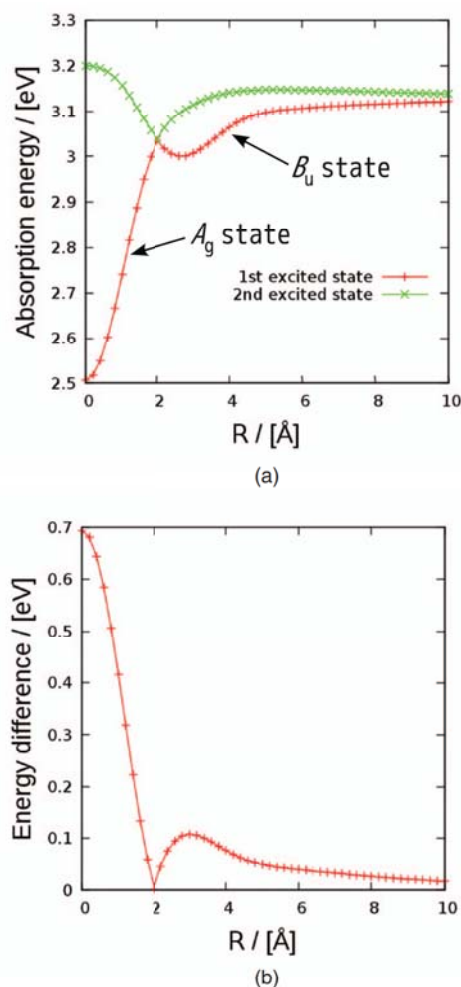


FIG. 5. (a) Absorption energies of tetracene dimer as a function of intermolecular distance and (b) difference in the absorption energies between the first and second excited states.

states, respectively. From these results, the dependence of the absorption energy on the intermolecular separation was confirmed to be caused by the change in orbital characters, as proposed by Kuzmaier *et al.*

We also calculated the oscillator strength as a function of the intermolecular separation, and the results are shown in Fig. 6. As found here, the oscillator strength for the first excited state was to be zero in the region of 0.0–2.0 Å, and suddenly it had non-zero values at more than 2.0 Å. On the contrary, the oscillator strength for the second excited state had non-zero values in the region of 0.0–2.0 Å, and became zero at more than 2.0 Å. From these results, the first and second excited states at less than 2.0 Å were interpreted as the forbidden and allowed transitions, respectively. In addition, these transition characters were found to be exchanged with each other at more than 2.0 Å. To investigate this reason, we analyzed the electronic structures of the excited states. As a result, the first and second excited states at less than 2.0 Å were to be the  $A_g$  and  $B_u$  states, respectively. Therefore, according to the selection rule,<sup>47</sup> the transition from the ground state to the first excited state was forbidden, and the transition to the second excited state was allowed. In contrast, the first and second



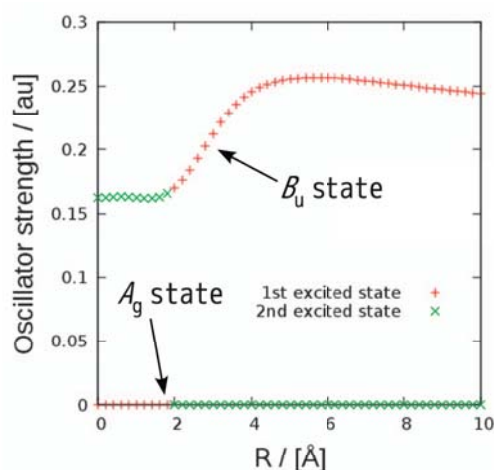


FIG. 6. Oscillator strength of tetracene dimer as a function of intermolecular distance.

excited states at more than 2.0 Å were to be the  $B_u$  and  $A_g$  states, respectively, which brought about the allowed and forbidden transitions for the first and second excited states, respectively. From these results, the order of energy levels of the  $A_g$  and  $B_u$  states was found to be important for the magnitude of the oscillator strength for the first and second excited states.

In common, the H and J aggregates are known to exhibit the absorption intensities originating from the second and first excited states, respectively.<sup>2,12</sup> Such features were observed also in the present calculations. As found from Figs. 4 and 6, the molecular displacement at 0.0 Å corresponded to the H aggregate, and the oscillator strength for the second excited state had a non-zero value. On the other hand, the increase in the intermolecular separation changed the molecular displacement from the H aggregate to the J aggregate, and the oscillator strength for the first excited state had non-zero values at more than 2.0 Å. Therefore, the present calculations successfully reproduced the features on the absorption intensities of the H and J aggregates. Hence, the molecular displacement could be identified as the H aggregate at less than 2.0 Å and as the J aggregates at more than 2.0 Å in the present system.

As shown in Secs. IV B and IV E, the calculated absorption energy of BUR was considerably red-shifted from that of BUY, and it was caused by the difference in the orbital characters. Since the present analysis clearly showed the relationship between the orbital character and the intermolecular separation, we also focused on the molecular displacements of BUR and BUY. For this purpose, we calculated the intermolecular distances of BUR and BUY, for which the dimer conformations 1 and 6 were used. As a result, the intermolecular distances of BUR and BUY were to be 3.2 Å and 4.0 Å, respectively. Applying these values to Fig. 5(a), the absorption energies were obtained to be 3.01 eV at 3.2 Å and 3.07 eV at 4.0 Å. Therefore, this analysis could qualitatively represent the spectral shift between BUR and BUY, although the absorption-energy curves in Fig. 5(a) were calculated with the tetracene dimer, not with the BUR and BUY ones. Here, we recall that the  $B_u$  state corresponded to the allowed transition

for the tetracene dimer. As shown in Fig. 5(a), the  $B_u$  state was to be the first excited state at more than 2.0 Å, and it had the energy minimum at around 3.0 Å. Therefore, the intermolecular distance of BUR was found to be closer to the energy minimum than that of BUY, and such a difference in the intermolecular distances caused the spectral shift between BUR and BUY. From these results, the intermolecular distance at the energy minimum of the  $B_u$  state was found to play a significant role in the spectral tuning.

## V. CONCLUSIONS

In this paper, we investigated the mechanism of crystallochromy on the red and yellow solids of tetracenes. The absorption and fluorescence energies calculated with the TDFI-TI method successfully reproduced the experimental values, which allowed us to explore the underlying molecular mechanism. As a result of the analysis, the largest contribution to the spectral shift was found to come from the difference in the multimerization effects between BUR and BUY. Although the side-chain conformational effect also provided a non-negligible contribution to the spectral shift, it was insufficient for reproducing the experimental value. In addition, the electrostatic solid-state effect was found to be very small. The further analysis of the calculated absorption energies clearly showed that the multimerization effect was mainly caused by the ET, HT, and CT interactions, not by the EET interaction. Therefore, the small contribution from the EET interaction was clarified in the present system, although the EET interaction is commonly considered as the main factor for the magnitude of electronic coupling. Based on these results, we also succeeded in understanding the reason for the failure in the absorption energy calculations performed in the previous study. Hence, we successfully showed the relationship between the orbital character and the spectral shift, which supported the pioneering work of Kazmaier and Hoffmann. To further investigate the mechanism of the crystallochromy, we analyzed the influence of the geometrical arrangement of the molecules. As a result, the excited state character was found to strongly depend on the molecular displacement. Such dependence had a large effect on the magnitudes of the absorption energy and oscillator strength, and hence the intermolecular distance at the energy minimum of the  $B_u$  state was found to play a significant role in the spectral tuning.

The present results indicated that the TDFI-TI calculation with the mcQM/MM optimized structure is a promising approach for studying the spectral tuning of the solid-state tetracenes. The TDFI-TI scheme can be combined with other electronic structure method, even though only the CIS, TD-rCAM-B3LYP, and SAC-CI methods were adopted in the present study. The high accuracy and the wide applicability of this approach will also enable one to analyze and understand other systems of crystallochromy.

## ACKNOWLEDGMENTS

This study was supported by MEXT KAKENHI Grant Nos. 23108709 and 23108720, and JSPS KAKENHI Grant No. 25810004.



- <sup>1</sup>G. Klebe, F. Graser, E. Hädicke, and J. Berndt, *Acta Crystallogr., Sect. B: Struct. Sci.* **45**, 69 (1989).
- <sup>2</sup>O. Valdes-Aguilera and D. C. Neckers, *Acc. Chem. Res.* **22**, 171 (1989).
- <sup>3</sup>A. Hantzsch, *Ber. Dtsch. Chem. Ges. B* **40**, 1533 (1907).
- <sup>4</sup>A. Hantzsch, *Angew. Chem.* **20**, 1889 (1907).
- <sup>5</sup>W. C. McCrone, in *Physics and Chemistry of the Organic Solid State*, edited by D. Fox, M. M. Labes, and A. Weissberger (Interscience, New York, 1965), p. 725.
- <sup>6</sup>H. de Diesbach and E. von der Weid, *Helv. Chim. Acta* **10**, 886 (1927).
- <sup>7</sup>E. A. Lucia and F. D. Verderame, *J. Chem. Phys.* **48**, 2674 (1968).
- <sup>8</sup>J. Bernstein and A. T. Hagler, *J. Am. Chem. Soc.* **100**, 673 (1978).
- <sup>9</sup>C. Reichardt, *Solvents and Solvent Effects in Organic Chemistry*, 3rd ed. (Wiley-VCH, Weinheim, 2003).
- <sup>10</sup>E. G. McRae and M. Kasha, *J. Chem. Phys.* **28**, 721 (1958).
- <sup>11</sup>E. E. Jelley, *Nature (London)* **138**, 1009 (1936).
- <sup>12</sup>M. Kasha, H. R. Rawls, and M. A. El-Bayoumi, *Pure Appl. Chem.* **11**, 371 (1965).
- <sup>13</sup>V. Czikkely, H. D. Försterling, and H. Kuhn, *Chem. Phys. Lett.* **6**, 207 (1970).
- <sup>14</sup>T. Nagamura and S. Kamata, *J. Photochem. Photobiol., A* **55**, 187 (1990).
- <sup>15</sup>J. Frenkel, *Phys. Rev.* **37**, 1276 (1931).
- <sup>16</sup>P. M. Kazmaier and R. Hoffmann, *J. Am. Chem. Soc.* **116**, 9684 (1994).
- <sup>17</sup>M. D. Newton, *Chem. Rev.* **91**, 767 (1991).
- <sup>18</sup>T. Förster, *Ann. Phys.* **437**, 55 (1948).
- <sup>19</sup>D. L. Dexter, *J. Chem. Phys.* **21**, 836 (1953).
- <sup>20</sup>R. D. Harcourt, G. D. Scholes, and K. P. Ghiggino, *J. Chem. Phys.* **101**, 10521 (1994).
- <sup>21</sup>C. Kitamura, Y. Abe, T. Ohara, A. Yoneda, T. Kawase, T. Kobayashi, H. Naito, and T. Komatsu, *Chem. Eur. J.* **16**, 890 (2010).
- <sup>22</sup>K. J. Fujimoto, *J. Chem. Phys.* **137**, 034101 (2012).
- <sup>23</sup>A. Warshel and W. W. Parson, *J. Am. Chem. Soc.* **109**, 6143 (1987).
- <sup>24</sup>G. D. Scholes, *ACS Nano* **2**, 523 (2008).
- <sup>25</sup>K. Fujimoto and W.-T. Yang, *J. Chem. Phys.* **129**, 054102 (2008).
- <sup>26</sup>K. J. Fujimoto and S. Hayashi, *J. Am. Chem. Soc.* **131**, 14152 (2009).
- <sup>27</sup>K. J. Fujimoto, *J. Chem. Phys.* **133**, 124101 (2010).
- <sup>28</sup>T. Koopmans, *Physica* **1**, 104 (1934).
- <sup>29</sup>V. Coropceanu, J. Cornil, D. A. da Silva Filho, Y. Olivier, R. Silbey, and J.-L. Brédas, *Chem. Rev.* **107**, 926 (2007).
- <sup>30</sup>P.-O. Löwdin, *J. Chem. Phys.* **18**, 365 (1950).
- <sup>31</sup>W. W. Parson, *Modern Optical Spectroscopy* (Springer-Verlag, Berlin, 2007).
- <sup>32</sup>M. D. Newton and N. Sutin, *Ann. Rev. Phys. Chem.* **35**, 437 (1984).
- <sup>33</sup>K. Huang and A. Rhys, *Proc. R. Soc. London, Ser. A* **204**, 406 (1950).
- <sup>34</sup>H. Bässler and B. Schweitzer, *Acc. Chem. Res.* **32**, 173 (1999).
- <sup>35</sup>Y. Kiyota, J. Hasegawa, K. Fujimoto, B. Swerts, and H. Nakatsuji, *J. Comput. Chem.* **30**, 1351 (2009).
- <sup>36</sup>W. Kohn and L. J. Sham, *Phys. Rev.* **140**, A1133 (1965).
- <sup>37</sup>C. Lee, W.-T. Yang, and R. G. Parr, *Phys. Rev. B* **37**, 785 (1988).
- <sup>38</sup>E. Runge and E. K. U. Gross, *Phys. Rev. Lett.* **52**, 997 (1984).
- <sup>39</sup>J. Wang, R. M. Wolf, J. W. Caldwell, P. A. Kollman, and D. A. Case, *J. Comput. Chem.* **25**, 1157 (2004).
- <sup>40</sup>J. B. Foresman, M. Head-Gordon, J. A. Pople, and M. J. Frisch, *J. Chem. Phys.* **96**, 135 (1992).
- <sup>41</sup>H. Nakatsuji, *Chem. Phys. Lett.* **59**, 362 (1978).
- <sup>42</sup>A. J. Cohen, P. Mori-Sánchez, and W.-T. Yang, *J. Chem. Phys.* **126**, 191109 (2007).
- <sup>43</sup>M. T. Cancès, B. Mennucci, and J. Tomasi, *J. Chem. Phys.* **107**, 3032 (1997).
- <sup>44</sup>M. W. Wong, *Chem. Phys. Lett.* **256**, 391 (1996).
- <sup>45</sup>J. W. Ponder, Tinker4.2, Washington University, St. Louis, MO, 2004.
- <sup>46</sup>M. J. Frisch, G. W. Trucks, H. B. Schlegel *et al.*, GAUSSIAN03, Gaussian, Inc., Pittsburgh, PA, 2003.
- <sup>47</sup>P. Atkins and R. Friedman, *Molecular Quantum Mechanics*, 5th ed. (Oxford University Press, New York, 2011).